



# Electronic properties of perovskite strontium chromium oxyfluoride epitaxial thin films fabricated via low-temperature topotactic reaction

著者	Akira Chikamatsu, Takahiro Maruyama, Tsukasa Katayama, Yu Su, Yoshihiro Tsujimoto, Kazunari Yamaura, Miho Kitamura, Koji Horiba, Hiroshi Kumigashira, Tetsuya Hasegawa
journal or publication title	Physical Review Materials
volume	4
number	2
page range	025004
year	2020-02-18
URL	<a href="http://hdl.handle.net/10097/00130780">http://hdl.handle.net/10097/00130780</a>

doi: 10.1103/PhysRevMaterials.4.025004

## Electronic properties of perovskite strontium chromium oxyfluoride epitaxial thin films fabricated via low-temperature topotactic reaction

Akira Chikamatsu <sup>1,\*</sup>, Takahiro Maruyama,<sup>1</sup> Tsukasa Katayama <sup>1</sup>, Yu Su,<sup>2</sup> Yoshihiro Tsujimoto,<sup>2,3</sup> Kazunari Yamaura,<sup>2,3</sup> Miho Kitamura,<sup>4</sup> Koji Horiba,<sup>4</sup> Hiroshi Kumigashira,<sup>4,5</sup> and Tetsuya Hasegawa<sup>1</sup>

<sup>1</sup>Department of Chemistry, The University of Tokyo, 7-3-1 Hongo, Bunkyo-ku, Tokyo 113-0033, Japan

<sup>2</sup>Research Center for Functional Materials, National Institute for Materials Science, 1-1 Namiki, Tsukuba, Ibaraki 305-0044, Japan

<sup>3</sup>Graduate School of Chemical Sciences and Engineering, Hokkaido University, North 13 West 8, Kita-ku, Sapporo 060-0808, Japan

<sup>4</sup>Institute of Materials Structure Science, High Energy Accelerator Research Organization (KEK), 1-1 Oho, Tsukuba, Ibaraki 305-0801, Japan

<sup>5</sup>Institute of Multidisciplinary Research for Advanced Materials, Tohoku University, 2-1-1 Katahira, Aoba-ku, Sendai 980-8577, Japan



(Received 17 October 2019; revised manuscript received 23 January 2020; accepted 31 January 2020; published 18 February 2020)

Perovskite chromium oxyfluoride  $\text{SrCrO}_{2.6}\text{F}_{0.4}$  epitaxial thin films were fabricated via low-temperature topotactic fluorination of  $\text{SrCrO}_{2.8}$  precursor with polyvinylidene fluoride as a fluorine source. The obtained  $\text{SrCrO}_{2.6}\text{F}_{0.4}$  thin film had a different chemical composition than that of bulk polycrystalline  $\text{SrCrO}_{2.8}\text{F}_{0.2}$ , possibly due to the higher reactivity of such thin film. Both the precursor and fluorinated thin films containing  $\text{Cr}^{3.6+}$  exhibited insulating behavior with band gaps of  $\sim 0.6$  eV, in contrast to metallic  $\text{SrCrO}_3$  with  $\text{Cr}^{4+}$  at 300 K. The experimentally observed valence and conduction bands of the  $\text{SrCrO}_{2.8}$ ,  $\text{SrCrO}_3$ , and  $\text{SrCrO}_{2.6}\text{F}_{0.4}$  thin films suggested that the spectral weight transfer from the coherent part to the incoherent part with the reduction of Cr valences was caused by strong electron correlation effects. This study offers a fundamental understanding of the fluorine doping effects on a crystalline structure and the correlated electronic performance of chromium oxides.

DOI: [10.1103/PhysRevMaterials.4.025004](https://doi.org/10.1103/PhysRevMaterials.4.025004)

### I. INTRODUCTION

Perovskite-type chromium oxides exhibit unique physical properties due to the strong Cr  $3d$ -O  $2p$  interaction. A typical example is  $\text{SrCrO}_3$  containing  $\text{Cr}^{4+}$  ( $3d^2$ ), where the Cr  $3d$  states split into  $t_{2g}$  and  $e_g$  orbitals and two valence electrons occupy the nearly triply degenerated  $t_{2g}$  orbitals [1–3]. Cubic  $\text{SrCrO}_3$  exhibits antiferromagnetic metallic behaviors because its transport property lies in the crossover region between itinerant and localized carriers [1,2]. Substituting  $\text{La}^{3+}$  for  $\text{Sr}^{2+}$  in  $\text{SrCrO}_3$  dopes electrons in the system and induces an electronic phase transition from antiferromagnetic metal to antiferromagnetic insulator [4–6]. Introduction of oxygen vacancies and insertion/substitution of  $\text{H}^-$  ions into  $\text{SrCrO}_3$  have been attempted to alter its electronic properties [7–9]. Cubic metallic  $\text{SrCrO}_3$  can be reversibly transformed into rhombohedral semiconducting  $\text{SrCrO}_{2.8}$  by changing the annealing atmosphere between vacuum ( $\text{SrCrO}_3 \rightarrow \text{SrCrO}_{2.8}$ ) and air ( $\text{SrCrO}_{2.8} \rightarrow \text{SrCrO}_3$ ) at relatively low temperatures (250–500 °C), as reported in the cases of epitaxial films and bulk polycrystals [7,8]. Rhombohedral  $\text{SrCrO}_{2.8}$ , which has {111}-oriented planes of  $\text{SrO}_2$  with adjacent layers of tetrahedrally coordinated  $\text{Cr}^{4+}$ , exhibits fast  $\text{O}^{2-}$  diffusion [7].  $\text{SrCrO}_2\text{H}$  synthesized by a high-pressure method is known to be an antiferromagnetic insulator with a Néel temperature ( $T_N$ ) of 380 K [9]. This  $T_N$  value is the highest among

chromium oxides and can be reasonably explained by the tolerance factor [9].

The physical properties of perovskite-type Cr oxides can be readily modified through topotactic fluorination because insertion or substitution of  $\text{F}^-$  ions provides additional holes or electrons to the Cr ions, respectively. For example, layered  $\text{La}_2\text{SrCr}_2^{4+}\text{O}_7\text{F}_2$  and nonlayered  $\text{SrCr}^{3.8+}\text{O}_{2.8}\text{F}_{0.2}$  have been synthesized in polycrystalline form by topotactic fluorination of  $\text{La}_2\text{SrCr}_2^{3+}\text{O}_7$  using  $\text{CuF}_2$  [10] and  $\text{SrCr}^{4+}\text{O}_3$  with polyvinylidene fluoride (PVDF) [11], respectively. These oxyfluorides exhibit antiferromagnetism with  $T_N$  of 140 and 230 K, respectively [10,11], which is much higher than that reported for  $\text{SrCrO}_3$  ( $T_N = 35$ –40 K) [12]. The fluoride ion substitution for the oxide ion sites would directly affect the connectivity of the Cr-anion network responsible for electrical conduction. However, electrical conduction characteristics and electronic states of perovskite-type Cr oxyfluorides have not yet been discussed.

In order to obtain the intrinsic electronic properties of perovskite-type Cr oxyfluorides, phase-pure and single-crystalline samples are desired. Use of epitaxial thin films as precursors for topotactic fluorination allows the preparation of such oxyfluoride samples in thin film form [13]. Indeed, PVDF-mediated topotactic fluorination reactions have been applied to various transition-metal oxide epitaxial thin films so far, such as  $\text{La}_{1-x}\text{Sr}_x\text{MnO}_{3-\delta}$ ,  $\text{SrFeO}_{3-\delta}$ ,  $\text{SrCoO}_{2.5}$ , (La, Nd) $\text{NiO}_3$ ,  $\text{BaBiO}_3$ , and layered  $\text{Sr}_2\text{RuO}_4$  [13–20]. In addition, thin-film samples are generally more reactive than bulk samples because of larger surface areas and smaller

\*chikamatsu@chem.s.u-tokyo.ac.jp

volumes [13]. Here, we report fluorine doping in perovskite-type  $\text{SrCrO}_{2.8}$  epitaxial thin films via topotactic fluorination using PVDF. We obtained perovskite-type  $\text{SrCrO}_{2.6}\text{F}_{0.4}$  epitaxial thin films, which had higher fluorine content than that in bulk polycrystalline  $\text{SrCrO}_{2.8}\text{F}_{0.2}$  [11]. Based on the results of resistivity and optical and electronic spectroscopy measurements, we discuss the transport properties and electronic structure of  $\text{SrCrO}_{2.6}\text{F}_{0.4}$  thin film in comparison with those of  $\text{SrCrO}_{2.8}$  and  $\text{SrCrO}_3$ . It offers a fundamental understanding of the fluorine doping effects on a crystalline structure and the correlated electronic performance of chromium oxides.

## II. EXPERIMENTAL

Precursor  $\text{SrCrO}_{2.8}$  thin films were grown on  $\text{LaAlO}_3$  (001) (LAO, Shinkosha Co.) substrates by pulsed-laser deposition (PLD) technique, using a KrF excimer laser (wavelength  $\lambda = 248$  nm) with an energy of  $1.5 \text{ J/cm}^2/\text{shot}$  and a repetition rate of 2 Hz. Polycrystalline  $\text{SrCrO}_3$  ceramic pellets used as PLD targets were synthesized using a high-pressure method. A stoichiometric mixture of SrO (prepared by heating  $\text{SrCO}_3$  at  $1300^\circ\text{C}$  in an  $\text{O}_2$  gas atmosphere) and  $\text{CrO}_2$  (Aldrich) was finely ground, then loaded into a Pt capsule, and placed in a high-pressure cell. This cell was then heated at 6 GPa and  $1000^\circ\text{C}$  for 1 h and then quenched to room temperature by turning off the heat before pressure was released. During each PLD run, the substrate temperature and oxygen partial pressure were set at  $750^\circ\text{C}$  and  $1 \times 10^{-7}$  Torr, respectively. The obtained  $\text{SrCrO}_{2.8}$  thin films were further subjected to fluorination using PVDF (Fluorochem Ltd.) under Ar gas flow at reaction temperatures ( $T_f$ ) of  $100 - 400^\circ\text{C}$  for 12 h. Following the methodology previously developed by our group [13,16,18–20], the films were covered with Al foil during fluorination to avoid the adhesion of the charcoal-like residue produced by the decomposition of the PVDF. The fluorinated films were rinsed with ethanol. Oxidized films were prepared by annealing the  $\text{SrCrO}_{2.8}$  precursor thin films at  $250^\circ\text{C}$  in air for 2 h. The typical thickness of the films was evaluated at  $\sim 50$  nm using x-ray reflectivity (Bruker AXS D8 DISCOVER).

Crystal structures of the films were characterized by x-ray diffraction (XRD, Bruker AXS D8 Discover) with Cu  $K\alpha$  radiation. Chemical compositions were determined using an energy-dispersive x-ray spectrometer (EDS, JEOL JED-2300) in conjunction with a scanning electron microscope (JEOL JSM-7100F), which was operated at an electron accelerating energy of 2.5 keV to reduce any substrate contribution. The depth profiles of the chemical compositions were analyzed by employing x-ray photoemission spectroscopy (XPS, JEOL JPS-9010MC) with  $\text{Ar}^+$ -ion etching. Surface morphology was characterized by atomic force microscopy (AFM, SII SPI4000). Cr  $2p$  and valence-band XPS and O  $K$ -edge x-ray absorption spectroscopy (XAS) spectra were measured at beamline BL-2A MUSASHI of the KEK-PF synchrotron facility. The Cr  $2p$  and valence-band XPS spectra were measured at 300 K using a VG-SCIENTA SES-2002 electron-energy analyzer with an energy resolution of 300 meV at a photon energy of 1200 eV. The Fermi level of the samples was set as that of an *in situ* evaporated gold foil which was in electrical contact with the sample. The O  $K$ -edge XAS spectra were measured at 300 K by the total-electron-yield method.

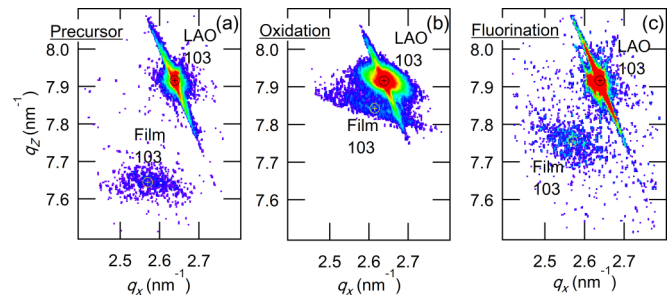


FIG. 1. Reciprocal space maps of the (a)  $\text{SrCrO}_{2.8}$  precursor film, (b) oxidized film, and (c) fluorinated film.

Before the synchrotron XPS and XAS measurements, the films were kept in a high-vacuum atmosphere ( $< 3 \times 10^{-7}$  Pa) for more than 2 h to remove surface gas contaminants as much as possible. In-plane electrical resistivities ( $\rho$ ) were measured by the four-terminal method with silver electrodes, using Physical Property Measurement System (Quantum Design Co.), in which the maximum measurement range for  $\rho$  was  $100 \Omega \text{ cm}$ . Optical spectra were measured at 300 K using an ultraviolet–visible–near-infrared (UV-Vis-NIR) spectrometer (Jasco V670DS) and a Fourier transform infrared spectrometer (FTIR, Jasco FT/IR-4600).

## III. RESULTS AND DISCUSSION

Fluorination of the  $\text{SrCrO}_{2.8}$  precursor thin film with PVDF was conducted at  $T_f = 200 - 350^\circ\text{C}$  (Supplemental Material, Fig. S1) [21]. Figure 1 shows reciprocal space maps around the 103 diffraction of the  $\text{SrCrO}_{2.8}$  precursor film, the oxidized film at  $250^\circ\text{C}$  in air, and the fluorinated film with PVDF at  $250^\circ\text{C}$  on the LAO substrates. The  $q_x$  values of the films were different from that of the LAO substrate, indicating that all the films were relaxed from the LAO substrates. No secondary phases were detected in any of the films in the angle range of  $10^\circ - 60^\circ$ , confirmed by the  $2\theta - \theta$  XRD patterns at a tilting angle of  $\chi = 90^\circ$  (Supplemental Material, Fig. S2) [21]. Note that the  $\text{SrCrO}_{2.8}$  precursor thin film had a tetragonal structure, as seen from the  $\varphi$  scan profile around the (103) reflection (Supplemental Material, Fig. S3) [21]. The  $a$ - and  $c$ -axes lengths of the precursor film were calculated as 0.389 and 0.392 nm, respectively, which were different from those of the strained  $\text{SrCrO}_{2.8}$  films ( $a = 0.382$  nm,  $c = 0.392$  nm) [7]. This discrepancy may be due to the difference in lattice strain and/or crystalline symmetry. After the oxidation, the  $a$ - and  $c$ -axes lengths decreased to 0.383 and 0.383 nm, respectively, possibly due to the increase of the valence number of the Cr ions. On the other hand, the  $a$ - and  $c$ -axes lengths of the fluorinated film were calculated as 0.389 and 0.387 nm, respectively, although these lengths are larger than those of bulk cubic  $\text{SrCrO}_{2.8}\text{F}_{0.2}$  ( $a = 0.3853$  nm) [11].

In order to examine the chemical composition of the films, EDS and XPS measurements were performed. Figure 2 shows the 2.5-keV EDS spectra of the  $\text{SrCrO}_{2.8}$  precursor and the fluorinated films, where the spectra were normalized by the area of the Sr  $L\alpha$  peak. The EDS spectra near O  $K\alpha$ , Cr  $L\alpha$ , and F  $K\alpha$  and the fitting results obtained by least-square fitting are shown in the inset of Fig. 2 and Fig. S4 [21], respectively.

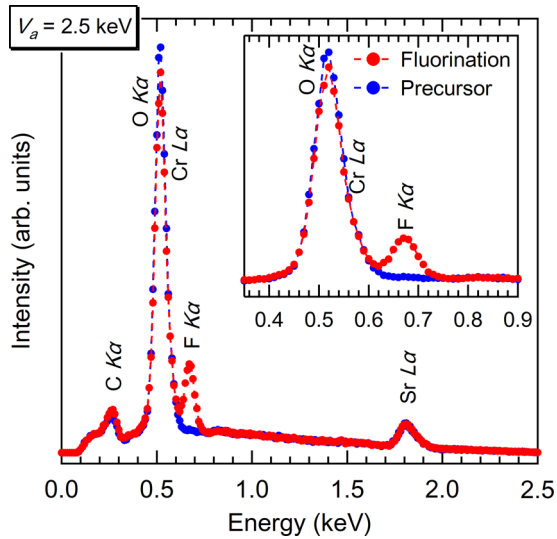


FIG. 2. 2.5-keV EDS results of the  $\text{SrCrO}_{2.8}$  precursor film (blue line) and the fluorinated films reacted with PVDF at  $250^\circ\text{C}$  for 12 h (red line). The inset shows a close-up near  $\text{O } K\alpha$ ,  $\text{Cr } L\alpha$ , and  $\text{F } K\alpha$ .

In the fluorinated film, an  $\text{F } K\alpha$  peak was observed with a concurrent decrease in the intensity of the  $\text{O } K\alpha$  peak, indicating that incorporation of fluorine into the anion sites and partial removal of oxygen took place simultaneously during the fluorination process. Figure 3 depicts the elemental depth profiles in the film fluorinated at  $250^\circ\text{C}$ , determined from the peak areas of the  $\text{F } 1s$ ,  $\text{Sr } 3d$ ,  $\text{Cr } 2p_{3/2}$ ,  $\text{La } 4d$ , and  $\text{Al } 2p$  measured by XPS combined with  $\text{Ar}^+$ -ion etching. As seen in Fig. 3, the signal intensity of F was almost constant at 5–40 nm and slightly increased near the interface between

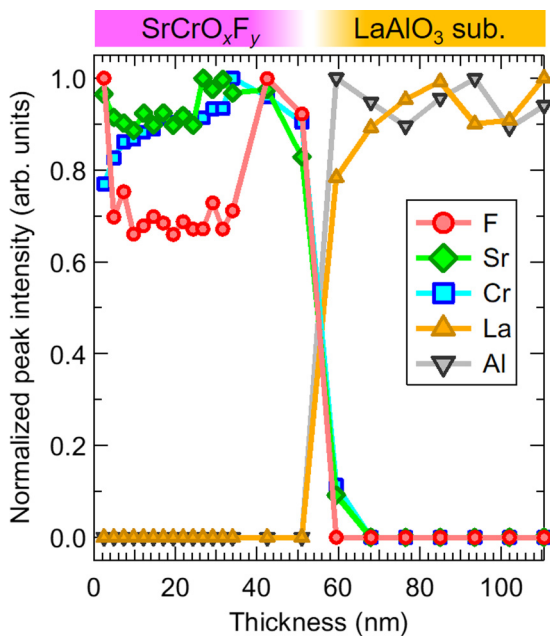


FIG. 3. Normalized concentration-depth profiles of the film fluorinated at  $250^\circ\text{C}$  obtained from the  $\text{F } 1s$  (red circle),  $\text{Sr } 3d$  (green diamond),  $\text{Cr } 2p_{3/2}$  (blue square),  $\text{La } 4d$  (orange triangle), and  $\text{Al } 2p$  (black inverted triangle) XPS spectra.

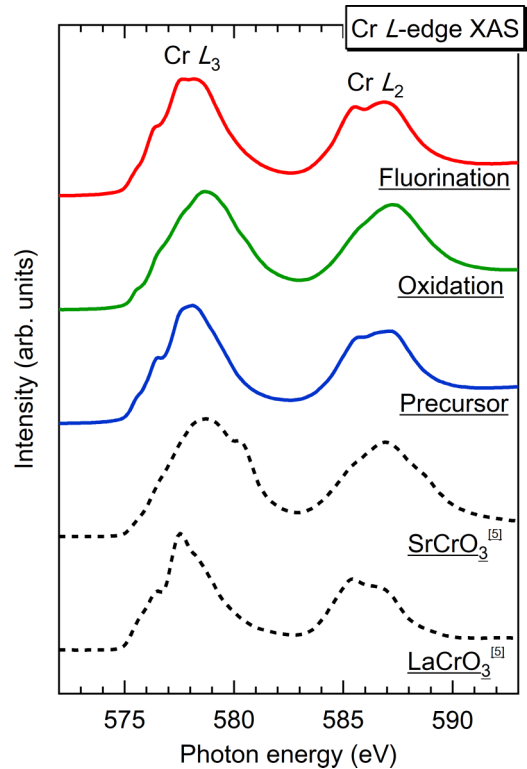


FIG. 4. Cr  $L$ -edge XAS spectra of the  $\text{SrCrO}_{2.8}$  precursor film (blue line), the oxidized film annealed at  $250^\circ\text{C}$  in air (green line), and the film fluorinated with PVDF at  $250^\circ\text{C}$  (red line). The reference spectra of  $\text{SrCrO}_3$  ( $\text{Cr}^{4+}$ ) and the  $\text{LaCrO}_3$  ( $\text{Cr}^{3+}$ ) are also shown in the figure.

the film and the substrate. These results suggest that the F ions diffused over the entire film. On the other hand, in the substrate region where the intensities of La and Al abruptly increased, F was not detected, indicating that the diffusion of F into the LAO substrate was negligible. Furthermore, the root-mean-square surface roughness values of the  $\text{SrCrO}_{2.8}$  precursor and fluorinated films were determined by AFM measurements to be 0.59 and 1.13 nm, respectively (Supplemental Material, Fig. S5) [21].

To examine the changes of the valence numbers of Cr by the oxidation and fluorination, we performed Cr  $L$ -edge XAS measurements, as shown in Fig. 4. It is known that the shape of Cr  $L$ -edge XAS spectrum of  $\text{Cr}^{4+}$  is very different from that of  $\text{Cr}^{3+}$  and that the valence number of Cr can be roughly estimated from the linear combination of  $\text{Cr}^{4+}$  and  $\text{Cr}^{3+}$  XAS spectra [22]. As seen in Fig. 4, the positions of the highest  $L_3$  and  $L_2$  peaks (578.7 and 587 eV) of the oxidized film were almost the same as those of the  $\text{SrCrO}_3$  reference, indicating that the oxidized film had  $\text{Cr}^{4+}$ . Thus, we determined the chemical formula of the oxidized film as  $\text{SrCrO}_3$ . Note that the peak at  $\sim 582$  eV was not observed in the oxidized film, which may be due to a change in Cr–O bond lengths associated with lattice strain and/or degraded crystallinity. On the other hand, the valence numbers of Cr in both precursor and fluorinated films were estimated to be  $3.6 \pm 0.1$  so as to reproduce the energy positions of the highest Cr  $L$ -edge peak by linearly combining the spectra of the oxidized

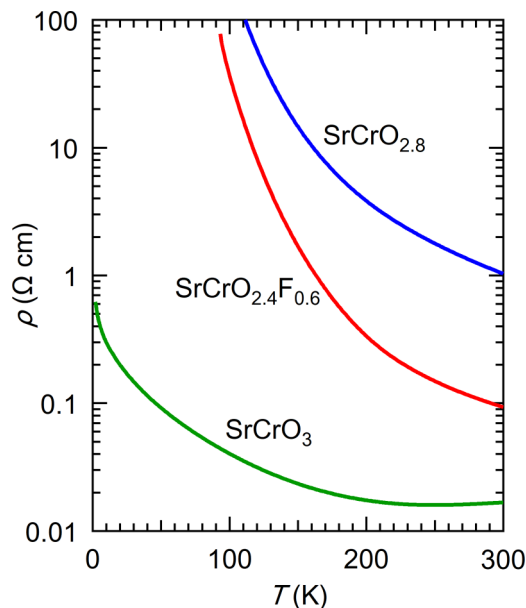


FIG. 5.  $\rho$ - $T$  curves for the  $\text{SrCrO}_{2.8}$  (blue line),  $\text{SrCrO}_{2.6}\text{F}_{0.4}$  (red line), and  $\text{SrCrO}_3$  (green line) films.

film ( $\text{Cr}^{4+}$ ) and  $\text{LaCrO}_3$  reference [5] ( $\text{Cr}^{3+}$ ) in Fig. S6 [21]. Assuming  $x + y = 3$  in  $\text{SrCrO}_x\text{F}_y$ , the chemical composition of the fluorinated film can be estimated as  $\text{SrCrO}_{2.6}\text{F}_{0.4}$ . Note that our fluorinated film had a higher fluorine content than polycrystalline bulk sample,  $\text{SrCrO}_{2.8}\text{F}_{0.2}$  [11], probably reflecting a higher reactivity of thin films than bulk because of larger surface areas and smaller volumes. Hereafter, the fluorinated film is referred to as  $\text{SrCrO}_{2.6}\text{F}_{0.4}$ .

Figure 5 plots the resistivity ( $\rho$ ) of the  $\text{SrCrO}_{2.8}$ ,  $\text{SrCrO}_3$ , and  $\text{SrCrO}_{2.6}\text{F}_{0.4}$  films as a function of temperature ( $T$ ). The  $\rho(300\text{ K})$  value of the  $\text{SrCrO}_{2.8}$  film was  $\sim 1.0\ \Omega\ \text{cm}$ , which is two orders of magnitude higher than that of the  $\text{SrCrO}_3$  film,  $\sim 1.7 \times 10^{-2}\ \Omega\ \text{cm}$ , and one order of magnitude higher than that of the  $\text{SrCrO}_{2.6}\text{F}_{0.4}$  film,  $\sim 9.3 \times 10^{-2}\ \Omega\ \text{cm}$ . The  $\rho$ - $T$  curve of the  $\text{SrCrO}_3$  film showed metallic behavior ( $d\rho/dT > 0$ ) in the range of 250–300 K. Notably, the  $\rho(300\text{ K})$  value and metal-insulator transition (MIT) temperature of the  $\text{SrCrO}_3$  film are higher than those of the fully strained  $\text{SrCrO}_3$  film, at  $1.3 \times 10^{-3}\ \Omega\ \text{cm}$  and 50 K, respectively [2], which is likely due to the differences in magnitude of the epitaxial strain and/or crystallinity. On the other hand, the  $\rho$ - $T$  curves of the  $\text{SrCrO}_{2.8}$  and  $\text{SrCrO}_{2.6}\text{F}_{0.4}$  films showed insulating behavior ( $d\rho/dT < 0$ ). These results indicate that  $\text{SrCrO}_3$  undergoes MIT by substituting F for O, similar to the MIT associated with the introduction of oxygen vacancies.

Next, we discuss how the electronic structure changes with fluorination. Figure 6 shows the optical absorption spectra [ $\alpha(\omega)$ ] of the  $\text{SrCrO}_{2.8}$  and  $\text{SrCrO}_{2.6}\text{F}_{0.4}$  films, as calculated using the relation  $\alpha(\omega) = -\ln[T(\omega)_{\text{film+LAOsubstrate}}/T(\omega)_{\text{LAOsubstrate}}]/t$ , where  $T(\omega)$  is the optical transmittance spectrum, and  $t$  is the thickness of the thin film. The UV-VIS-IR transmittance and reflectivity spectra of the  $\text{SrCrO}_{2.8}$  and  $\text{SrCrO}_{2.6}\text{F}_{0.4}$  films and LAO substrate are shown in Supplemental Material, Fig. S7 [21]. As seen in Fig. 6, the  $\text{SrCrO}_{2.6}\text{F}_{0.4}$  film exhibited

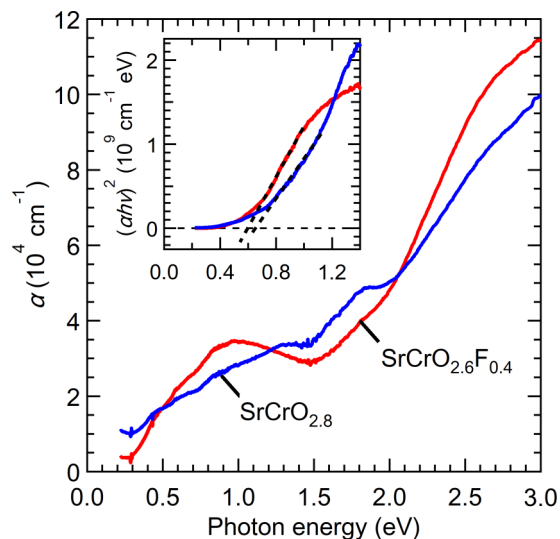


FIG. 6. Optical absorption spectra of the  $\text{SrCrO}_{2.8}$  (blue line) and  $\text{SrCrO}_{2.6}\text{F}_{0.4}$  films (red line). The inset plots the  $(\alpha h\nu)^2$  vs  $h\nu$  curves.

absorption peaks at 1 and 2.7 eV. In a semiconductor, the optical coefficient is known to follow the relation  $(\alpha h\nu)^n = A(h\nu - E_g)$  near the band edge, where  $E_g$  is the energy band gap,  $h\nu$  is the photon energy, and  $n$  is 2 for direct band gap or 1/2 for indirect band gap. The absorption spectra of both  $\text{SrCrO}_{2.8}$  and  $\text{SrCrO}_{2.6}\text{F}_{0.4}$  could be adequately fitted by  $(\alpha h\nu)^2$  rather than  $(\alpha h\nu)^{1/2}$ , suggesting that they have direct band gaps. The inset of Fig. 6 shows the  $(\alpha h\nu)^2$  vs  $h\nu$  curves for the two films. By extrapolating the linear portions of the curves to  $(\alpha h\nu)^2 = 0$ , the optical band-gap values are evaluated as  $\sim 0.6\ \text{eV}$  for both  $\text{SrCrO}_{2.8}$  and  $\text{SrCrO}_{2.6}\text{F}_{0.4}$ .

The electronic structures of the valence and conduction bands were probed by synchrotron XPS and O  $K$ -edge XAS measurements. Figure 7(a) shows the valence-band XPS

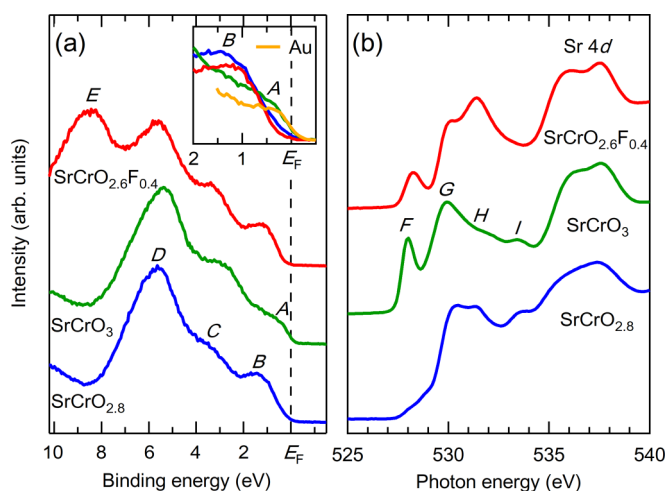


FIG. 7. (a) Valence-band XPS spectra of the  $\text{SrCrO}_{2.8}$  (blue line),  $\text{SrCrO}_3$  (green line), and  $\text{SrCrO}_{2.6}\text{F}_{0.4}$  films (red line). The inset of (a) shows the valence-band spectra close to the Fermi level, along with the spectrum from Au foil for energy calibration purposes (gold line). (b) O  $K$ -edge XAS spectra of the  $\text{SrCrO}_{2.8}$  (blue line),  $\text{SrCrO}_3$  (green line), and  $\text{SrCrO}_{2.6}\text{F}_{0.4}$  films (red line) measured at  $\theta_{\text{inc}} = 60^\circ$ .

spectra of the SrCrO<sub>2.8</sub>, SrCrO<sub>3</sub>, and SrCrO<sub>2.6</sub>F<sub>0.4</sub> films. The valence-band spectrum of the SrCrO<sub>2.8</sub> film mainly consists of three structures, labeled as *B*, *C*, and *D*. According to previous density-functional theory (DFT) calculations and XPS measurements [2], the structures *B*, *C*, and *D* can be assigned as incoherent parts of the Cr 3*d* *t*<sub>2*g*</sub>, O 2*p* nonbonding, and O 2*p* bonding bands, respectively. In the SrCrO<sub>3</sub> film, the structures *C* and *D* are rigidly shifted to lower binding energies by 0.25 eV, thereby representing the chemical-potential shift associated with electron doping. Near the Fermi level ( $E_F$ ), as shown in the inset of Fig. 7(a), the structure *B* was suppressed and a coherent part of Cr 3*d* *t*<sub>2*g*</sub> (structure *A*) evolved owing to the strong electron correlation effects, similar to other strongly correlated metallic transition-metal oxides, such as SrVO<sub>3</sub>, La<sub>1-*x*</sub>Sr<sub>*x*</sub>MnO<sub>3</sub>, and Ca<sub>1-*x*</sub>Sr<sub>*x*</sub>RuO<sub>3</sub> [23–25]. On the other hand, in the SrCrO<sub>2.6</sub>F<sub>0.4</sub> film, a gap opened at  $E_F$  and the structure *B* was enhanced, which was consistent with the insulating behavior of the SrCrO<sub>2.6</sub>F<sub>0.4</sub> film. The positions of the structures *C* and *D* were the same as those of the SrCrO<sub>2.8</sub> film, which was consistent with the XAS results, showing that SrCrO<sub>2.8</sub> and SrCrO<sub>2.6</sub>F<sub>0.4</sub> films had the same Cr valence numbers. In addition, a spectral structure *E* appeared around the binding energy of 7–10 eV. Considering higher electronegativity of fluorine than oxygen, the structure *E* is assignable to the F 2*p* bonding states.

Figure 7(b) shows the O *K*-edge XAS spectra of the SrCrO<sub>2.8</sub>, SrCrO<sub>3</sub>, and SrCrO<sub>2.6</sub>F<sub>0.4</sub> films measured using linearly polarized light, where the angle between the incident beam and the surface normal ( $\theta_{\text{inc}}$ ) was set at 60°. The O *K*-edge XAS spectra correspond to transitions into unoccupied O 2*p* states hybridized with Cr 3*d* and Sr 4*d*. As seen in Fig. 7(b), the peaks at 527–534 eV and those at 534–540 eV can be assigned to the Cr 3*d*-derived states (structures *F*, *G*, *H*, and *I*) and Sr 4*d*-derived states, respectively, by comparing the O *K*-edge XAS spectrum of the SrCrO<sub>3</sub> film [5]. Referring to the reported DFT calculations of SrCrO<sub>3</sub> and CrO<sub>2</sub> [2,26], we assigned the structure *F* to excitations of the unoccupied *t*<sub>2*g*</sub> ↑ band, the structures *G* and *H* to the combination of unoccupied *e*<sub>*g*</sub> ↑ and *t*<sub>2*g*</sub> ↓, and the structure *I* to the unoccupied *e*<sub>*g*</sub> ↓ band. The structure *F* of the SrCrO<sub>2.6</sub>F<sub>0.4</sub> film is located at 528.3 eV, which is 0.3 eV higher than that of the SrCrO<sub>3</sub> film. This suggests spectral weight transfer from the coherent part to the

incoherent part with fluorination due to strong electron correlation effects. Moreover, the peak intensity of the structure *F* of the SrCrO<sub>2.6</sub>F<sub>0.4</sub> film was smaller than that of the SrCrO<sub>3</sub> film. This is mainly due to the decrease in Cr valence number, as seen in the case of La<sub>1-*x*</sub>Sr<sub>*x*</sub>CrO<sub>3</sub> thin films [5]. On the other hand, the SrCrO<sub>2.6</sub>F<sub>0.4</sub> film showed a larger intensity than the SrCrO<sub>2.8</sub> film, although the Cr valence numbers were the same. This may be due to local distortion of Cr–O bonds, because XAS using linearly polarized light is sensitive to the angle between the incident beam and the axes of O 2*p* orbitals due to the dipole selection rule [27].

#### IV. CONCLUSION

We fabricated chromium oxyfluoride epitaxial thin films by PVDF-mediated fluorination of SrCrO<sub>2.8</sub> precursor and investigated the effects of fluorine doping on the electronic properties. After reacting with PVDF, the SrCrO<sub>2.8</sub> precursor film grown on an LAO substrate was transformed into SrCrO<sub>2.6</sub>F<sub>0.4</sub>, and its fluorine content was higher than that of bulk polycrystalline SrCrO<sub>2.8</sub>F<sub>0.2</sub>, hence reflecting the higher reactivity of thin films. The  $\rho$ -*T* curves of the SrCrO<sub>2.8</sub> and SrCrO<sub>2.6</sub>F<sub>0.4</sub> films with Cr<sup>3.6+</sup> showed insulating behavior, which was in stark contrast to SrCrO<sub>3</sub> with Cr<sup>4+</sup> exhibiting metallic transport properties at 300 K. The optical  $E_g$  values of the SrCrO<sub>2.8</sub> and SrCrO<sub>2.6</sub>F<sub>0.4</sub> were evaluated as ~0.6 eV by UV-VIS-IR measurements. The results of XPS and XAS measurements suggested spectral weight transfer from the coherent part to the incoherent part, accompanied by the reduction of Cr valences from Cr<sup>4+</sup> to Cr<sup>3.6+</sup> due to strong electron correlation effects. These findings can help understand the fluorine doping effects on crystalline and electronic structures of unknown chromium oxyfluorides.

#### ACKNOWLEDGMENTS

This work was supported by Japan Society for the Promotion of Science (JSPS) KAKENHI Grants No. JP15H02024, No. JP16H06438, No. JP16H06441, and No. JP19H02594. Synchrotron radiation experiments were performed with the approval of the Photon Factory Program Advisory Committee, KEK (Proposals No. 2017G557 No. and 2018S2-004).

- [1] A. C. Komarek, S. V. Streltsov, M. Isobe, T. Möller, M. Hoelzel, A. Senyshyn, D. Trots, M. T. Fernández-Díaz, T. Hansen, H. Gotou, T. Yagi, Y. Ueda, V. I. Anisimov, M. Grüninger, D. I. Khomskii, and M. Braden, *Phys. Rev. Lett.* **101**, 167204 (2008).
- [2] K. H. L. Zhang, Y. Du, P. V. Sushko, M. E. Bowden, V. Shutthanandan, L. Qiao, G. X. Cao, Z. Gai, S. Sallis, L. F. J. Piper, and S. A. Chambers, *J. Phys.: Condens. Matter* **27**, 245605 (2015).
- [3] Z. H. Zhu, F. J. Rueckert, J. I. Budnick, W. A. Hines, M. Jain, H. Zhang, and B. O. Wells, *Phys. Rev. B* **87**, 195129 (2013).
- [4] K. Maiti and D. D. Sarma, *Phys. Rev. B* **54**, 7816 (1996).
- [5] K. H. L. Zhang, Y. Du, P. V. Sushko, M. E. Bowden, V. Shutthanandan, S. Sallis, L. F. J. Piper, and S. A. Chambers, *Phys. Rev. B* **91**, 155129 (2015).
- [6] K. H. L. Zhang, Y. Du, A. Papadogianni, O. Bierwagen, S. Sallis, L. F. J. Piper, M. E. Bowden, V. Shutthanandan, P. V. Sushko, and S. A. Chambers, *Adv. Mater.* **27**, 5191 (2015).
- [7] K. H. L. Zhang, P. V. Sushko, R. Colby, Y. Du, M. E. Bowden, and S. A. Chambers, *Nat. Commun.* **5**, 4669 (2014).
- [8] A. M. Arévalo-López, J. A. Rodgers, M. S. Senn, F. Sher, J. Farnham, W. Gibbs, and J. P. Attfield, *Angew. Chem. Int. Ed.* **51**, 10791 (2012).
- [9] C. Tassel, Y. Goto, Y. Kuno, J. Hester, M. Green, Y. Kobayashi, and H. Kageyama, *Angew. Chem. Int. Ed.* **53**, 10377 (2014).
- [10] R. Zhang, G. Read, F. Lang, T. Lancaster, S. J. Blundell, and M. A. Hayward, *Inorg. Chem.* **55**, 3169 (2016).

- [11] Y. Su, Y. Tsujimoto, K. Fujii, Y. Masubuchi, H. Ohata, H. Iwai, M. Yashima, and K. Yamaura, *Chem. Commun.* **55**, 7239 (2019).
- [12] L. O.-S.-Martin, A. J. Williams, J. Rodgers, J. P. Attfield, G. Heymann, and H. Huppertz, *Phys. Rev. Lett.* **99**, 255701 (2007).
- [13] T. Katayama, A. Chikamatsu, Y. Hirose, R. Takagi, H. Kamisaka, T. Fukumura, and T. Hasegawa, *J. Mater. Chem. C* **2**, 5350 (2014).
- [14] P. A. Sukkurji, A. Molinari, C. Reitz, R. Witte, C. Kübel, V. S. K. Chakravadhanula, R. Kruk, and O. Clemens, *Materials* **11**, 1204 (2018).
- [15] J. Wang, Y. Shin, E. Arenholz, B. M. Lefler, J. M. Rondinelli, and S. J. May, *Phys. Rev. Mater.* **2**, 073407 (2018).
- [16] T. Katayama, A. Chikamatsu, Y. Hirose, T. Fukumura, and T. Hasegawa, *J. Sol-Gel Sci. Technol.* **73**, 527 (2015).
- [17] E. J. Moon, Y. Xie, E. D. Laird, D. J. Keavney, C. Y. Li, and S. J. May, *J. Am. Chem. Soc.* **136**, 2224 (2014).
- [18] T. Onozuka, A. Chikamatsu, T. Katayama, Y. Hirose, I. Harayama, D. Sekiba, E. Ikenaga, M. Minohara, H. Kumigashira, and T. Hasegawa, *ACS Appl. Mater. Interfaces* **9**, 10882 (2017).
- [19] A. Chikamatsu, K. Kawahara, T. Shiina, T. Onozuka, T. Katayama, and T. Hasegawa, *ACS Omega* **3**, 13141 (2018).
- [20] K. Kawahara, A. Chikamatsu, T. Katayama, T. Onozuka, D. Ogawa, K. Morikawa, E. Ikenaga, Y. Hirose, I. Harayama, D. Sekiba, T. Fukumura, and T. Hasegawa, *CrystEngComm* **19**, 313 (2017).
- [21] See Supplemental Material at <http://link.aps.org/supplemental/10.1103/PhysRevMaterials.4.025004> for  $2\theta - \theta$  XRD patterns at  $\chi = 90^\circ$ ,  $\varphi$  scan around the (103) reflection, 2.5-keV EDS results, AFM images, Cr *L*-edge XAS linear spectra, and UV-VIS-IR transmittance and reflectivity spectra.
- [22] H.-J. Noh, J.-S. Kang, S. S. Lee, G. Kim, S.-W. Han, S.-J. Oh, J.-Y. Kim, H.-G. Lee, S. Yeo, S. Guha, and S.-W. Cheong, *Europhys. Lett.* **78**, 27004 (2007).
- [23] M. Takizawa, M. Minohara, H. Kumigashira, D. Toyota, M. Oshima, H. Wadati, T. Yoshida, A. Fujimori, M. Lippmaa, M. Kawasaki, H. Koinuma, G. Sordi, and M. Rozenberg, *Phys. Rev. B* **80**, 235104 (2009).
- [24] A. Chikamatsu, H. Wadati, H. Kumigashira, M. Oshima, A. Fujimori, M. Lippmaa, K. Ono, M. Kawasaki, and H. Koinuma, *Phys. Rev. B* **76**, 201103(R) (2007).
- [25] M. Takizawa, D. Toyota, H. Wadati, A. Chikamatsu, H. Kumigashira, A. Fujimori, M. Oshima, Z. Fang, M. Lippmaa, M. Kawasaki, and H. Koinuma, *Phys. Rev. B* **72**, 060404(R) (2005).
- [26] C. B. Staggarescu, X. Su, D. E. Eastman, K. N. Altmann, F. J. Himpsel, and A. Gupta, *Phys. Rev. B* **61**, R9233 (2000).
- [27] M. Schmidt, T. R. Cummins, M. Bürk, D. H. Lu, N. Nücker, S. Schuppler, and F. Lichtenberg, *Phys. Rev. B* **53**, R14761 (1996).